AFRL-SR-AR-TR-06-0019

REPORT DOCUMENTATION PAGE

1. REPORT DATE (DD-MM-YYYY) 12-01-2006	2. REPORT TYPE Final report	3. DATES COVERED (From - To) 4/01/2004 to 9/30/05

4. TITLE AND SUBTITLE	5a. CONTRACT NUMBER
Single Molecule Detection Using a Silicon Nanopore-Nanotransistor Integrated Circuit	
	5b. GRANT NUMBER
	FA9550-04-1-0214
	5c. PROGRAM ELEMENT NUMBER

6. AUTHOR(S)	5d. PROJECT NUMBER
G. Timp, J.P. Leburton, N. Aluru, and K. Schulten	
	5e. TASK NUMBER
	5f. WORK UNIT NUMBER

7. PERFORMING ORGANIZATION NAME(S) AND ADDRESS(ES)	8. PERFORMING ORGANIZATION REPORT NUMBER
University of Illinois	

9. SPONSORING / MONITORING AGENCY NAME(S) AND ADDRESS(ES)	10. SPONSOR/MONITOR'S ACRONYM(S)
Air Force Office of Hugh DeLong Scientific Research	
	11. SPONSOR/MONITOR'S REPORT NUMBER(S)

12. DISTRIBUTION / AVAILABILITY STATEMENT

Approve for PUblic Release: Distribution Unlimited

20060131 283

13. SUPPLEMENTARY NOTES

14. ABSTRACT

The focus of program was the production and testing of the transducer that consists of a nanopore integrated with a MOSFET amplifier. The essential component is a single, nanometer-diameter pore in a robust, nanometer-thick membrane formed from a Metal Oxide Semiconductor (MOS) capacitor about $2\mu m$ on edge. When an electric field is applied across the membrane immersed in electrolyte, a polyanion (like *DNA*) injected at the negative electrode is attracted to the pore, blocks the ion current, and under certain conditions translocates through it. As the molecule permeates the capacitor membrane through the pore, the electrostatic charge distribution associated with the nucleotides comprising the *DNA* polarizes the capacitor and induces a voltage on the electrodes that is measured with an on-chip amplifier. For the analysis of these signals and the identification of a unique molecular signature, we will relied on molecular dynamics simulations to provide us with an atomically accurate appraisal of the forces, charge distributions and voltages that develop during a translocation.

15. SUBJECT TERMS

16. SECURITY CLASSIFICATION OF:			17. LIMITATION OF ABSTRACT	18. NUMBER OF PAGES	19a. NAME OF RESPONSIBLE PERSON
a. REPORT	b. ABSTRACT	c. THIS PAGE			19b. TELEPHONE NUMBER (include area code)

Standard Form 298 (Rev. 8-98)
Prescribed by ANSI Std. Z39.18

Executive Summary:

The focus of program was the production and testing of the transducer r that consists of a nanopore integrated with a MOSFET amplifier. The essential component is a single, nanometer-diameter pore in a robust, nanometer-thick membrane formed from a Metal Oxide Semiconductor (MOS) capacitor about $2\mu m$ on edge. When an electric field is applied across the membrane immersed in electrolyte, a polyanion (like *DNA*) injected at the negative electrode is attracted to the pore, blocks the ion current, and under certain conditions translocates through it. As the molecule permeates the capacitor membrane through the pore, the electrostatic charge distribution associated with the nucleotides comprising the *DNA* polarizes the capacitor and induces a voltage on the electrodes that is measured with an on-chip amplifier. For the analysis of these signals and the identification of a unique molecular signature, we will relied on molecular dynamics simulations, to provide us with an atomically accurate appraisal of the forces, charge distributions and voltages that develop during a translocation. As shown below, we have demonstrated the operation of the separate components: i.e. we have studied ssDNA translocating through a <1.5nm pore in a 45nm thick MOS capacitor membrane; we have fabricated and tested a 1millisecond molecular trap; we have fabricated and tested a broad-band low noise MOSFET amplifier with a 290GHz cut-off frequency (Figure 1(e)) and we have calibrated MD simulations through measurements of the voltage threshold predicted or *dsDNA* for pores ranging from 0.9 to 1.5nm-radius. In this program, working with Lucent Technologies through the New Jersey Nanotechnology Consortium, we planned to integrate these components together into a scalable, robust, low noise transducer that is sensitive to the electronic structure a single, specific molecule. The footprint for this chip would be less than 1millimeter on edge.

Team Member Organization(s):

The UIUC team consists of: Profs. Klaus Schulten, Jean-Pierre Leburton and Narayana Aluru,
Two post-docs: Maria Gracheva and Alek Aksimentiev
Graduate Students: Jiunn Heng, Val Dimitrov, Oelena Dimauro, Chuen Ho

The NJNC team consists of: Bill, Mansfield, Avi Kornblit, Fred Klemens, Tom Sorsch and John Miner

Publications:

1. J.B. Heng, A. Aksimentiev, C. Ho, P. Marks, Y.V. Grinkova, S. Sligar, K. Schulten, and **G. Timp**, *The Electromechanics of DNA in a Synthetic Nanopore*, to be published Biophys. J. (2005).
2. V. Dimitrov, J. B. Heng, K. Timp, O. Dimauro, R. Chan, J. Feng, W. Hafez, T. Sorsch, W. Mansfield, J. Miner, A. Kornblit, F. Klemens, J. Bower, R. Cirelli, E. Ferry, A. Taylor, M. Feng, and **G. Timp**, *High Performance, sub-50nm MOSFETS for Mixed Signal Applications*, IEDM Tech. Digest, 2005.
3. C. Ho, R. Qiao, J. Heng, A. Chatterjee, R. Timp, N. Aluru, and **G. Timp**, *Electrolytic Transport Through a Synthetic Nanometer-diameter Pore*, Proceedings National Academy of Sciences, 102(30) 10445-10450, 2005.
4. J.B. Heng, A. Aksimentiev, C. Ho, P. Marks, Y.V. Grinkova, S. Sligar, K. Schulten, and **G. Timp**, *Stretching DNA using the Electric Field in a Synthetic Nanopore*, NanoLetters 5(10); 1883-1888 (2005).
5. J.B. Heng, C. Ho, T. Kim, R. Timp, A. Aksimentiev, Y.V. Grinkova, S. Sligar, K. Schulten, and **G. Timp**, *Sizing DNA Using a Nanometer-Diameter Pore*, Biophys. J., 87: 2905-2911, (2004).
6. A. Aksimentiev, J.B. Heng, **G. Timp**, and K. Schulten, *Microscopic Kinetics of DNA Translocation through Synthetic Nanopores*, Biophys. J. 87: 2086-2097 (2004).

Objectives:

We plan to produce, test and simulate the performance of 1-10nm diameter pores through 10-65 nanometer-thick membranes fabricated from MOS-capacitors to explore their use for sequencing a single DNA molecule.

Technical Approach:

To determine the chemical sequence of a single DNA molecule, we intend to measure the dipole moment induced in the capacitor by each nucleotide as the molecule is electrophoretically driven across the membrane through the nanopore. We also plan a hierarchy of simulations and measurements, in concert, to establish the accuracy of MD simulations of nanopores, which will be used to predict the performance and optimize the sensor design. First, the ionic conductivity through the pore was measured and compared with the results of multi-scale simulations that are used to compute I-V characteristics, using molecular dynamic (MD) simulations to account for the charge in the pore, the structure and viscosity of the water, and reduced ion mobility. Second, we will accomplish simulations and measurements of permeation of nanopores by DNA that block the pore in the membrane. And third, simulations and experiments will focus on the detection of the voltage associated with the translocation of short *DNA* <100-mer through the nanopore in an MOS capacitor.

Accomplishments/Milestones:

The focus of program was the production and testing of the transducer represented schematically in Figure 1(a) that consists of a nanopore integrated with a MOSFET amplifier. The essential component is a single, nanometer-diameter pore (Figure 1(c)) in a robust, nanometer-thick membrane formed from a Metal Oxide Semiconductor (MOS) capacitor (Figure 1(b)) about 2μm on edge. When an electric field is applied across the membrane immersed in electrolyte, a polyanion (like *DNA*) injected at the negative electrode is attracted to the pore, blocks the ion current, and under certain conditions translocates through it. As the molecule permeates the capacitor membrane through the pore, the electrostatic charge distribution associated with the nucleotides comprising the *DNA* polarizes the capacitor and induces a voltage on the electrodes that is measured with an on-chip amplifier. For the analysis of these signals and the identification of a unique molecular signature, we will rely on molecular dynamics simulations (Figure (1d)), to provide us with an atomically accurate appraisal of the forces, charge distributions and voltages that develop during a translocation. As shown below, we have demonstrated the operation of the separate components: i.e. we have studied ssDNA translocating through a <1.5nm pore in a 45nm thick MOS capacitor membrane; we have fabricated and tested a 1millisecond molecular trap; we have fabricated and tested a broad-band low noise MOSFET amplifier with a 290GHz cut-off frequency (Figure 1(e)) and we have calibrated MD simulations through measurements of the voltage threshold predicted
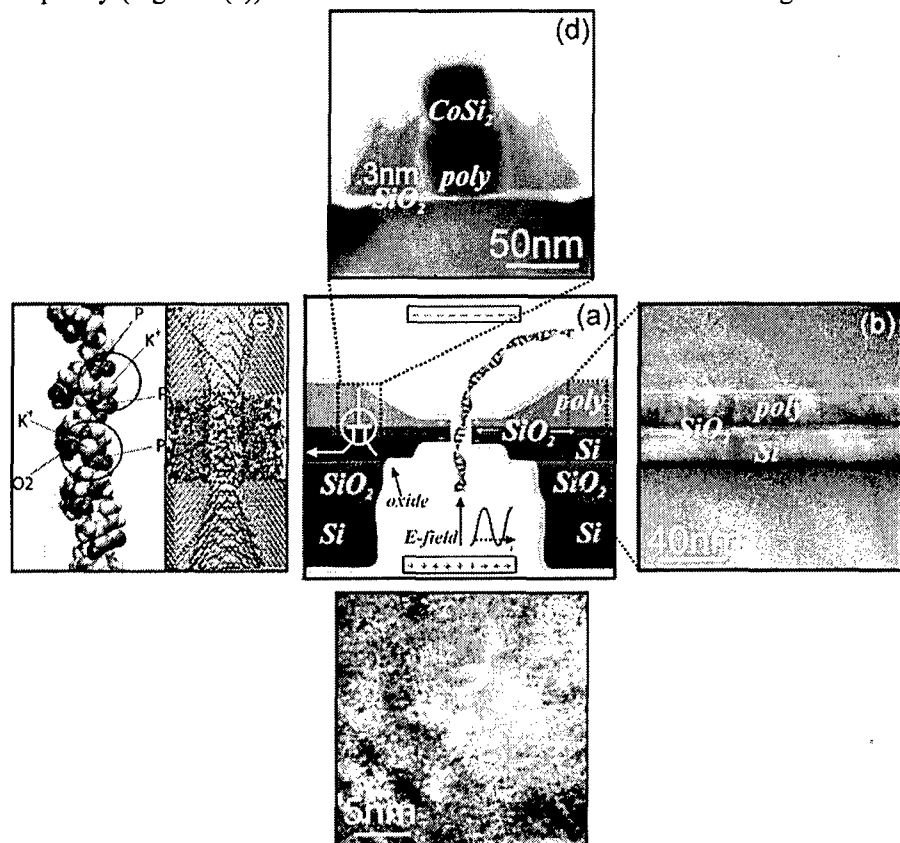

FIGURE 1. The Nanopore Transducer. (a) At the center of the figure is a schematic of a new type of bio-sensor that integrates a ~1nm diameter pore in a membrane formed from an MOS capacitor sequencing a single biomolecule. At the core of the proposed research is the demonstrated capability to produce ~1nm diameter pores in an ultra-thin MOS capacitor membrane. A STEM micrograph of a 1nm diameter pore in a capacitor membrane is shown in (b). A TEM micrograph of the capacitor-membrane consisting of heavily doped SOI layer is 22nm thick, and a heavily doped polysilicon layer 18nm thick sandwiching an SiO₂ membrane 4.2nm thick is shown in (c). According to our proposal, this nanopore mechanism works like a molecular trap. Feedback control of the longitudinal field in conjunction with the elastic properties of DNA is used to trap the molecule. Once the molecule is captured by the pore, feedback and a rotating transverse field trap it and an oscillating longitudinal field forces it to move back-and-forth between the capacitor electrodes facilitating synchronous detection. The signal between the electrodes is amplified using a high-speed low noise transistor amplifier integrated with the nanopore (d). To interpret the data, we plan to use a combination of molecular dynamics and nanometer-scale simulations to predict the voltage distribution self-consistently. An example of a "snap-shot" taken from a molecular dynamic calculation of single-stranded DNA in a 1nm pore is shown on the left in (e).

. for *dsDNA* for pores ranging from 0.9 to 1.5nm-radius. In this program, working with Lucent Technologies through the New Jersey Nanotechnology Consortium, we planned to integrate these components together into a scalable, robust, low noise transducer that is sensitive to the electronic structure a single, specific molecule. The footprint for this chip would be less than 1millimeter on edge.

We tested the efficacy of using synthetic nanopores for molecular detection of *DNA* using *pH* to affect the charge on the molecule; some of the results have been reported elsewhere.[57,3] For example, Fig. 2(a) shows the I-V characteristic through the same 0.5±0.1nm-radius pore, measured in the range ±1V in *1M KCl* electrolyte after >22hrs of immersion in de-ionized water. We measured the dc electrolytic current through the pore as a function of the applied electrochemical potential in a membrane transport bi-cell with each cell containing a volume of *KCl* electrolyte and a *Ag-AgCl* electrode. A constant voltage bias is applied between the electrodes and then a steady-state current is measured using an Axopatch 200B amplifier with a 10kHz bandwidth. Notice that the current is approximately a linear function of the voltage over the range (which is ~8x larger than voltages typically employed in measurements of α-hemolysin.) Subsequently, we tried using nanopores for molecular detection by injecting *DNA* along with *TRIS-EDTA* buffer (pH 8.0) into 1M *KCl* electrolyte near the negative electrode. While monitoring the ionic current through the pore under an applied bias, we observed transients associated with single *DNA* molecules temporarily blocking the electrolytic current through the pore. Figure 2(b) shows a continuous time sequence (blue) of the current through the 0.5nm-radius pore observed for an applied bias of 200mV after injecting 50-mer poly (dT) (poldeoxythymidylate) single-stranded *DNA* (*ssDNA*) at the negative electrode. The trace exhibits five current transients. In the same figure, there is a separate (red) trace corresponding to the baseline

measured without *DNA* at the negative electrode for comparison. We only observe transients after injecting the *DNA* at the negative electrode; if the *DNA* is inserted at the positive *AgCl* electrode instead, we do not observe such transients. Figure 2(c) is an expanded view of four representative time sequences illustrating transients associated with 50-mer poly (dT) *ssDNA* blocking the ionic current through the same R_p =0.5nm pore observed for an applied bias of 200mV (i-iii) and 500mV(iv). Poly (dT) was chosen because the effect of the secondary structure on the blockade current is expected to be minimal.[120] In each instance, the open current (120pA for 200mV and 320pA for 500mV) through the pore is blocked for only a limited time. Because of the low concentration of the *ssDNA* (~20μg/mL~33pmole/mL) in the electrolyte, and the small pore volume (~20nm³), we suppose that each of these electrical signatures is indicative of a single molecule interacting with the pore.

While the *ssDNA* blockades shown in Figure 2(c) are reminiscent of those induced by the same molecule in a α-hemolysin (Kasianowicz et al., 2001), we find that the duration, shape and magnitude of the blocking current vary stochastically and depend on the applied voltage. Unlike Kasianowicz, we do not generally observe distinct, two-level transitions between an open current through the pore and a well-defined blockade level. We have explored elsewhere through deconvolution the possibility that these differences might be attributed, in part, to the impulse response of the system consisting of the nanopore, the membrane and the apparatus used for the measurements, which is well represented by a 100μsec pulse. But with or without deconvolution, it is evident from the variety of transients observed that the level of the blocking
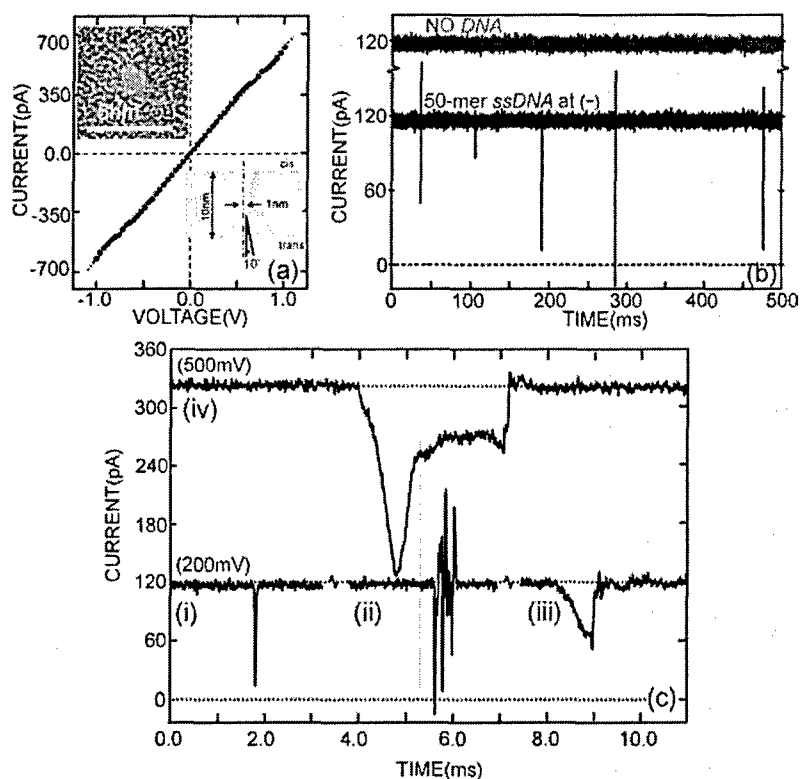

Figure 2. Characterization of Nanopore and Translocation of DNA.[57] The upper inset to Fig.(a) is a *TEM* image of a nanopore (slightly out of focus to exaggerate the pore) in a nominally 10 nm thick nitride membrane viewed at $0°$ tilt angle. The apparent diameter of the pore is 1.0±0.2nm. The lower inset is a schematic representation of the structure inferred from tilted *TEM* images of similar pores. The current-voltage characteristic of the nanopore is approximately linear. Figure (a) is a measurement of the I-V characteristic obtained in 1M *KCl* , corresponding to the nanopore shown in the inset. The fit through the data (red dashed line) has a slope of 0.63±0.03nS. When *DNA* is inserted at the negative electrode, transients are observed in the ionic current through the nanopore associated with a blockade by *DNA*. Figure (b) shows the current through the same nanopore as a continuous function of time with 50mer poly(dT) *ssDNA* inserted at the negative electrode (blue) and without it (red). Corresponding to the observation of transients, *DNA* is found at the positive electrode. Figure (c) illustrates the variety of transients observed in the same pore for an applied voltage of 200mV(i,ii,iii) and 500mV(iv) all plot on the same linear scale, but each transient has been offset for clarity. The blocking current is observed to vary during the transient, and from transient to transient as well. The width of the transients ranges from the bandwidth-limited 100μsec to 10msec.

. current changes during the time interval of the transient, which we interpret as the molecule interacting with the pore.

To quantitatively identify the forces, predict that electrical signals and estimate the noise associated with the translocation of *DNA* through the nanopore transducer with atomic resolution, we constructed a microscopic model of the experimental system and simulated electrophoretic transport through nanopore ranging in radius from 0.5nm to 1.5nm by using molecular dynamics. We inferred the shape of the nanopores from TEM and STEM images. Subsequently, by applying external electric fields, we simulated the field-driven translocations of *ssDNA* and *dsDNA* through pores. A crystalline Si_3N_4 membrane was built by replicating a unit cell of β-Si_3N_4 crystal along the unit cell vectors, producing a hexagonal patch of 10.3 nm thickness and 4.6 nm sides. By removing atoms from the Si_3N_4 patches we produced pores of symmetric double-conical (hourglass) shapes with radii that correspond to our experiments. Moreover, *DNA* with the exact same sequence as that used in our experiments was built from individual base pairs in the geometry suggested by Quanta.[11] The strand was placed in front of the pore, normal to the membrane. The Si_3N_4/*DNA* complex was then solvated in a volume of pre-equilibrated TIP3 water molecules. K^+ and Cl^- ions were added, corresponding to a concentration of 1M. The final system measured about 30.3nm in the direction normal to the Si_3N_4 membrane and included about 160,000 atoms. In order to simulate the *DNA*/nanopore system, molecular force field describing water, ions and nucleic acids[12] was combined with MSXX molecular force field for Si_3N_4[13]; the protocols are described in detail elsewhere.[10]

According to MD, the time required for *DNA* to transit the pore can be less than a microsecond. Furthermore, since they represent a complete accounting of the forces, these simulations represent an (optimistic) assessment of the bandwidth and noise performance that can be achieved with the simple *DNA*/nanopore microsystem studied experimentally. In the 50ns simulation shown in Figure 3, we observed translocation of a short *dsDNA* d(polyC)$_{20}$ through a pore of 1.2±0.1nm radius in a Si_3N_4 membrane 5.2nm thick, driven by an electric field of 8.7×10^7 V/m. (This field was purposefully chosen to be 14x higher than the experimental value to reduce the duration of the simulation.) Figure 3 illustrates a translocation, depicting the position of the *DNA* center of mass (blue) and the ionic current through the pore (black). The vertical dashed line indicates the moment when *DNA* was introduced into the simulation. The horizontal dashed line indicates the open pore ionic current found in the absence of *DNA*. Within the first few nanoseconds of the simulation, the electric field captures four pairs of nucleotides nearest to the aperture and drives them into the pore. The rest of the molecule moves down the pore following the charged backbone of the first few nucleotides, almost completely blocking the current. After 5ns, the *DNA* reaches the narrowest part of the pore and slows down. We observed a rupture of the hydrogen bonds connecting the bases of the three terminal base-pairs inside the pore, followed by a partial unzipping of the *DNA*. Two of the six non-bound bases adhere to the surface of the pore and remain in one location for an extended time interval (5-30ns). Subsequently, near t=42ns, we find a characteristic positive spike above the open pore current that correlates with the exit of *DNA* from the pore. When *DNA* exits the pore, ions accumulating near the mouth are also released resulting in the positive spike in the current. Although similar to those spikes observed experimentally on the rising edge of the current transients, the observed spikes could also be interpreted in terms of the impulse response of the nanopore-measurement system.

These simulations also indicate that the level of the %blocking current is correlated to the velocity of the molecule through the pore.[10] Consequently, we expect that interactions between the molecule, the pore, and the membrane give rise to a non-uniform molecular velocity and bulk electrolyte flow, which are manifested as variations in the blocking current during a single translocation. By using the nanopore as a stochastic sensor, measuring the % blocking current and the width of the blocking current transients, it may be possible to discriminate between polymers of different length. In particular, the prospects for sequencing *DNA* using blockade currents has already been methodically examined by Kasianowicz and others using a proteinaceous nanopore, α-hemolysin, as the prototype, but so far the primary structure associated with individual nucleotides has not been resolved. **First of all, there are limitations that are inherent to α-hemolysin nanopore.** For example, there are at least 20 nucleotides that lie within the lumen of the α-hemolysin pore during the translocation event and molecular dynamical simulations suggest that a large fraction of them contact the lumen wall.[11] The lipid bilayer is yet another limitation. This restriction is especially onerous because the molecules that we would like to identify exhibit a secondary structure that prevents (among other things) an unequivocal identification of the primary structure. The molecules of interest, like polynucleotides, form double helices. To unravel the secondary structure of a molecule it could be advantageous to increases the temperature or varying pH or pressure. While, bilayers formed from dipalmitoylphsphatidylcholine survive to 50C,[5] this is no guarantee that the channel protein will not denature. Another of the disadvantages is the fragility of the fused protein-membrane mechanism. The lipid bilayer membrane, which is usually suspended over a Teflon orifice, is typically 25-100μm in diameter and only 5nm thick. It ruptures after a few hours of use or after cycling the electrolyte a few times. The maximum sustained pressure differential is given by $\Delta P=2\tau_{LYS}/a$, where a is the diameter of the aperture and τ_{LYS} is the linear rupture strength of the lipid which varies from 5 to 30 dyne/cm. A 1-2μm diameter aperture will support only about 0.1 atmosphere but a 100nm diameter could support 2.3 atmospheres. Thus, nano-scale apertures (ranging from 10nm to 1μm in diameter) might be more robust and less susceptible to defects and tears. The smallest aperture that has been covered with a bilayer is ~30nm in diameter *in silicon*. **Second, how do we deconvolve the primary structure from the blockade current?** While it may be

possible to extract the underlying primary structure from a noisy local measurement of the electrical properties of the molecule[114] using computational methods[144] provided that the noise is minimal, the transfer rate through the pore is comparable to the bandwidth of the measurement apparatus and that high fidelity reference data is available/can be obtained, but so far this strategy has not succeeded.

One of the most severe limitations is associated with bandwidth and noise in the measurement of the blockade current. While it is possible to differentiate one long strand of homonucleotide *DNA* from another type by measuring the level of the blocking current, the rapid rate of translocation through the pore, coupled with the narrow bandwidth and noise in the measurement, preclude single nucleotide resolution in a polynucleotide. Most of the experimental work using a nanopore as a transducer for single molecule detection uses electronics borrowed from patch clamping, and so an analysis of the operation of a conventional patch clamp amplifier reveals the bandwidth and noise limitations of the measurement. A patch clamp measures the ion flux through nanopore by placing the tip of a glass pipette, drawn to a tip diameter of a few micrometers, in close proximity to a membrane. The glass pipette is filled with an electrolytic solution up to the bulk of a metal electrode, which is positioned a few millimeters above the channel. The metal electrode is fed into low-noise amplifier that uses a (Ge) JFET input stage. The relatively long column of electrolyte between the channel and the metal electrode in a conventional patch clamp, in conjunction with the small diameter of the pipette, gives rise to a high series resistance R_p, and capacitance C_p, that compromises the performance in several ways. The most important of these is the noise contribution of the pipette, which can often dominate total noise. For example, under optimal conditions, the noise contribution of the pipette is expected to be ~30-50 fA-rms in a 10 kHz bandwidth, and this would increase to
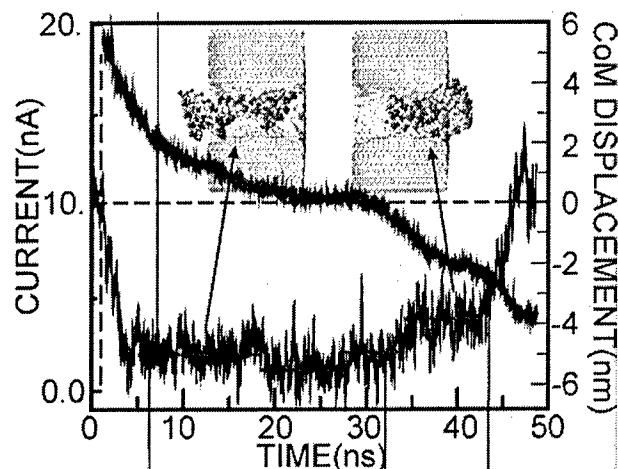

FIGURE 3. Molecular Dynamic Simulations of a Translocation. Simulations of the ion current through a nanopore in a silicon nitride membrane reveal that the current is substantially blocked as the molecule translocates through the pore. The figure shows the ion current and *DNA* displacement obtained from a simulation in which the axis of the molecule is aligned with the pore axis. The vertical dashed line indicates the time at which the DNA molecule is introduced into the system. The open pore current (in the absence of a *DNA* molecule) is indicated by the horizontal dashed line. The electric field is 1.4V/5.2nm, which is 14x larger than that used in the experiments, to economize on simulation time. Notice that the duration of the translocation is only about 45ns, and it ends with a positive current spike above the open pore current. The system configurations at 12ns and 40ns are indicated in the insets.

more than 10 pA-rms in a 500 kHz bandwidth; both of these figures are increased by a factor of ~3 under typical conditions. The noise contribution of the patch pipette and the origins of this noise have been extensively described[116] and will not be elaborated here. The pipette resistance, which is typically $R_p \sim$ 2-10 MΩ (or more), also has a detrimental effect on the dynamic response because it is in series with the patch capacitance C_m, which for most biological membranes is about 10fF/ m². For a patch area between 2-50 µm², C_m falls in the range of 0.02 to 0.5pF, with the lowest values of C_m associated with the highest values of R_p. Thus, the dynamic response of a conventional patch clamp is limited by the pipette resistance and patch capacitance to less than $\tau = R_p C_m \approx 1$µsec. In addition to that produced by the pipette, there are several other sources of noise that are of great importance to a patch clamp measurement, and severely limit its overall performance. Of primary importance is the noise of the input amplifier itself (a current-to-voltage converter). Present-day patch clamp amplifiers all rely on conventional JFETs (Junction Field Effect Transistors) for the input stage. If g_m is the transconductance of the FET front end in a conventional patch clamp, then the input voltage noise e_n is given by: $e_n^2 \sim 4kT$ g_m, where $\not{A}$ s an ideality factor that is usually larger than 0.67 (~1 is probably typical). A useful figure of merit for the ~10 m gate length JFETs currently employed in a patch clamp is the ratio of the transconductance to input capacitance, $g_m/C_{in} \approx 10^9$ s^{-1}, where C_{in} is the input capacitance of the FET. Thus for $C_{in} \approx 5$ pF, e_n can be estimated to be ~2 nV/√Hz. e_n combines with C_{in} and any other capacitance in series with the FET gate to produce current noise, i_n^2 that increases with frequency, f, as f^2. The other capacitances (denoted here by the lumped value C_e) in a traditional patch clamp consists of the capacitance of the pipette, input connector, 'reset' circuitry, 'compensation' capacitor, strays, etc., and can easily total 5pF. Thus $i_n^2 = 4\pi^2 e_n^2 (C_{in} + C_e)^2 f^2 \approx 1.5 \times 10^{-38} f^2$ (units: amp²/Hz). Rms-noise in a bandwidth B (Hz) from this source is given by $\{\frac{4}{3}\pi^2 c_2 e_n^2 (C_{in} + C_e)^2 B^3\}^{1/2}$, where c_2 is a coefficient that depends on the type of filter used to establish the bandwidth B ($c_2 \approx 2$ for an 8-pole Bessel filter). This is expected to amount to ~0.1 pA-rms in a 10 kHz bandwidth and ~35 pA rms in a 500 kHz bandwidth; the best existing patch clamp amplifier exhibits higher noise in this situation.

Another source of noise that is usually insignificant in present-day patch clamping – but which will become important in the improved techniques we propose *due to the minimization of other noise sources* is the thermal voltage noise of the access resistance, R_p, to the membrane patch (presently the patch pipette resistance) in series with the patch capacitance

C_m. The thermal voltage noise of R_p is given by $e_p{}^2 = 4kTR_p$, and the current noise arising from R_p and C_m is given by $i_p{}^2=4\pi^2 e_p{}^2 C_m{}^2 f^{\,2}$. Even if C_m is very small, the high resistance makes this 'R_p-C_m' noise potentially significant; nevertheless, the other sources of noise described above are usually much larger so that this source is only rarely important in present-day patch clamping. In the new techniques proposed here R_p will be greatly reduced, thus significantly reducing this source of noise. However, as described below, other sources of noise are expected to be reduced so dramatically due to miniaturization that this small but unavoidable source of noise will take on greater importance.

From the above analysis, we appreciate the significance that device capacitance and bandwidth have for the noise specification: smaller capacitance and narrow bandwidth improve the noise in the current blockade measurement. But with the limitations imposed by the capacitance of the membrane, in combination with the fragility of the lipid bilayer membrane, the limited aperture associated with the complex structure of the protein comprising the pore, the challenges inherent to re-engineering it, and the limited voltage and temperature range of operation, indicate that -hemolysin may not be a practical basis for a sequencing technology.

Despite all the shortcomings, electrical detection of a single molecule has several advantages. For example, for that case of DNA if each nucleotide has a characteristic signature, then a nanopore sensor could facilitate the analysis of the data by eliminating the need for sensitive dyes, thereby improving the dynamic range for detection. Moreover, a nanopore sensor might identify and measure the concentration at the same time sampling only a few molecules; single molecule sensitivity has already been demonstrated. Moreover, several analytes might be identified concurrently using a single nanopore sensor. And finally, electrical detection using a nanopore has the potential to move sequencing out of the lab into the clinic or the environment.

As an alternative to the measurement of the blockade current, we propose to use a generalized impedance measurement that reflects the local charge distribution in the molecule. This is accomplished using electrodes positioned on either side of the ultra-thin membrane. As illustrated in Figure 4, the membrane is formed on an SOI (silicon-on-insulator) substrate using conventional silicon processing technology. As shown in Figure 4(a), the capacitor electrodes that constitute the membrane are fabricated from heavily doped layers of silicon, appropriately thinned using a combination of oxidation and CMP (chemical-mechanical polishing). The insulator in the capacitor is formed by growing a nitrided-oxide on crystalline silicon using rapid thermal oxidation at 1000°C. The thickness of the SiO_2 insulator separating the electrodes forming the capacitor is a crucial specification. The spatial resolution for sequencing is essentially determined by the SiO_2 thickness. We have already produced oxides as thin as 0.7nm, but the measured leakage current due to quantum mechanical tunneling between
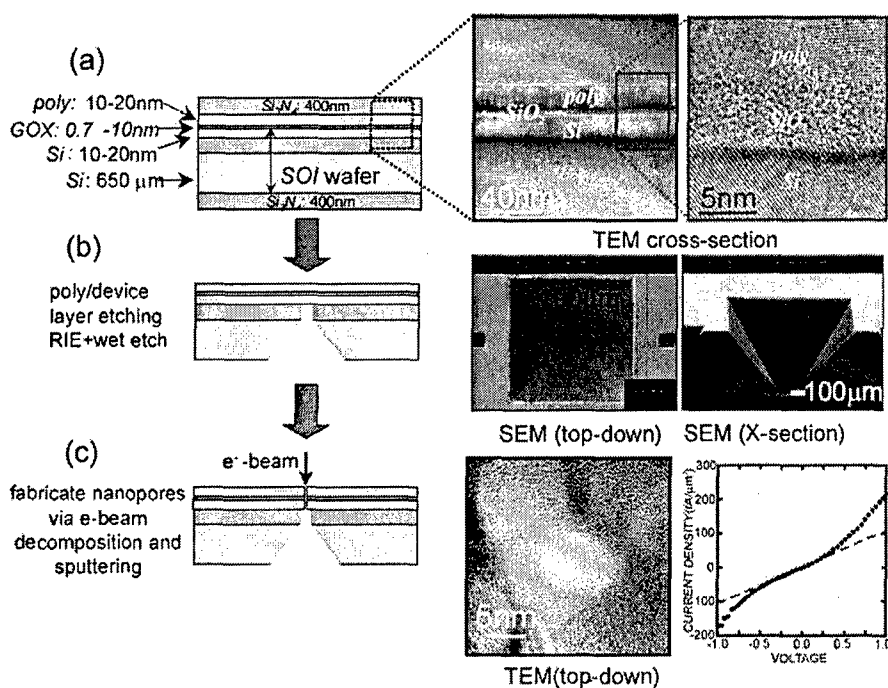

FIGURE 4. Fabrication Process for Producing Pores in a Nanometer-thick Capacitor. (a) The membranes are formed by depositing a gate oxide and polysilicon layer onto a thinned SOI susbtrate. A TEM cross-section through the membrane structure is shown on the right of (a). Using DUV lithography and a combination of wet and dry etching a membrane is revealed as illustrated in (b). Two SEM micrographs of the through-wafer via is shown in the right of (b). After revealing the membrane, a pore is subsequently, produced using electron beam decomposition and sputtering (c). A TEM micrograph of a ~8nm diameter pore is shown on the right, along with tunneling current measured after the pore has been sputtered through the capacitor.

the electrodes for 1V operation is about $3\mu A/\mu m^2$.[140] While the leakage current grows exponentially with decreasing oxide thickness, it also decreases exponentially with the operating voltage, so this level of current does not necessarily preclude the use of an oxide that is 0.7nm thick. However, to facilitate fabrication and avoid tunneling, we have been using a thicker 4-5nm thick oxide for the preliminary work as shown below. Once the layers that constitute the membrane have been formed, we use deep-UV lithography in conjunction with reactive ion and wet chemical etching to define the capacitor. Subsequently, the membrane is revealed using a through-wafer etch. The via associated with the through-wafer etch is shown in Figure 4(b) While the size of the membrane will ultimately be determined using microlithography to be 2μmx2μm, according to the design rules we intend to employ, for our preliminary work we used very large area membranes (100μmx100μm) to economize on time and cost.

To satisfy the stringent requirements for the manufacture of the capacitor-membranes, we collaborated with the New Jersey Nanotechnology Consortium (NJNC), a division of Lucent Technologies, which operates a state-of-the-art silicon processing facility in Murray Hill, NJ. After the membranes are formed at NJNC, the wafers are transported to the University of Illinois following a strict protocol to avoid contamination and damage, where the pores are sputtered. A single pore is created in each membrane through electron beam stimulated decomposition and sputtering using a JEOL2010F transmission electron microscope (STEM) operating at 200keV (with a field emission source), taking advantage of a tightly focused beam as small as 0.5nm (Gaussian width) in diameter. To guarantee the integrity of the membrane after a pore is sputtered through it, we measure the leakage current before and after sputtering. We cannot detect a difference in the leakage current in the voltage range <1V. Notice that a 500mV, the leakage current is <100fA/μm^2, which is about 100x smaller than the (unloaded) rms-noise specification given for the patch clamp amplifier used to measure blockade current.

Capacitance measurements are used routinely in the semiconductor industry to measure the charge distribution in MOS capacitors with high sensitivity. Heuristically, (in one-dimension) from Poisson's equation we expect that the voltage difference between the two electrodes will be proportional to the first moment of the charge distribution:

$$\delta V \sim \frac{1}{\varepsilon_{eff}\varepsilon_0}\sum_i x_i \rho(x_i) \sim \frac{1}{\varepsilon_{eff}\varepsilon_0}\int_0^{d_{ox}} x\rho(x)dx$$

where position variable x_i ranges over the thickness of the oxide from bottom of the top electrode to the top of the other, (x_i) represents the partial charge distribution within the pore (the charge associated with each atom comprising the molecule, the ions, the water, etc.) and ε_{eff} is the effective dielectric constant within the pore. So, measurements of the voltage might be used to extract information about the molecular charge distribution exposed during a translocation provided that: 1. there is sufficient signal-to-noise and 2. thermal motion and screening by ions and water do not obscure it.

Adopting this strategy, we have measured the voltage and current signals corresponding to the translocation of a single *dsDNA* molecule through a structure similar to that shown in Figure 1, consisting of a thin 4.2nm oxide sandwiched between two heavily doped (n-type) electrodes: one made from polysilicon 18nm thick and another from crystalline silicon 22nm thick. A 3.5nm-radius pore was made from polysilicon 18nm thick and another from crystalline silicon 22nm thick. A 3.5nm-radius pore was sputtered in this MOS-capacitor and the membrane was then inserted into a transport bi-cell made from PDMS, with each cell containing a 75μL volume of *KCl* electrolyte and a *Ag-AgCl* electrode. Once the ionic current between the *AgCl* electrodes through the nanopore stabilized, we injected 150bp poly(A)•poly(T) dsDNA along with *TRIS-EDTA* buffer (pH 8.0) into 1M *KCl* electrolyte near the Ag-AgClanode. While monitoring the ionic current through the pore under an applied bias between the *AgCl* electrodes of 200mV, we observed transients associated with single ds*DNA* molecules temporarily blocking the electrolytic current through the pore similar to those shown in Figure 5(a). Concurrent with the transients observed in the current, we recorded the voltage on the SOI and polysilicon electrodes, as well, using a Multiclamp 700B (Axon, Union City, CA) amplifier with a 50kHz bandwidth with multiple matched headstages. We did not always observe a signature above the noise on both the polysilicon and the SOI electrode in correspondence with the observation of a transient event in the current.
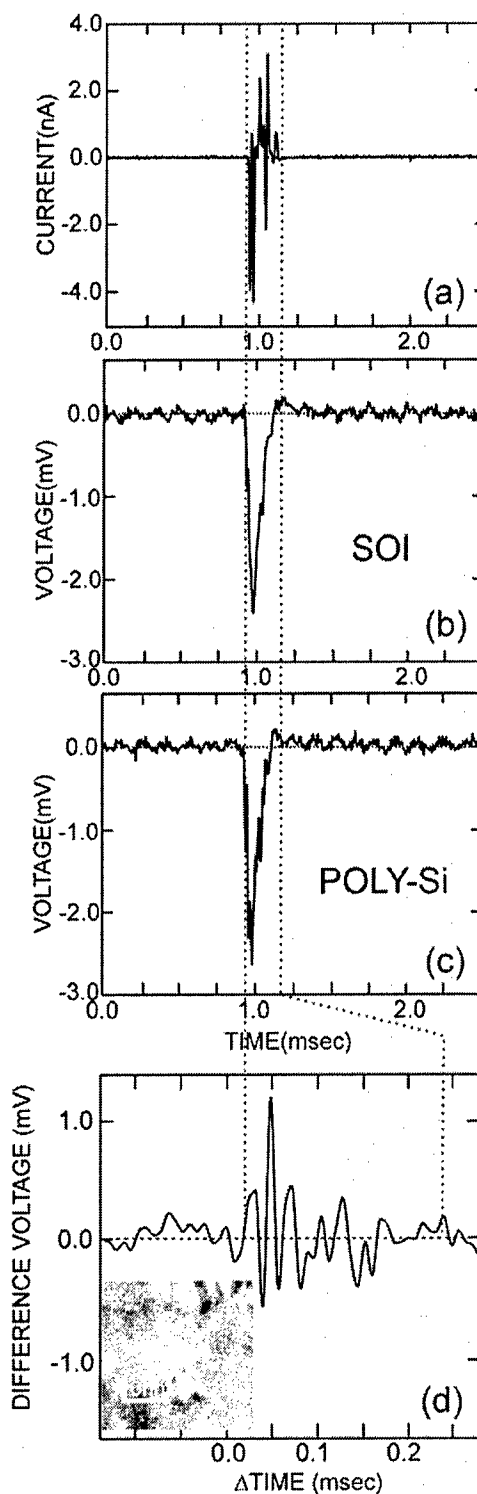

FIGURE 5. **Translocation through a 3.5nm Radius Pore in a Capacitor**. Corresponding to a transient in the current (a), we observe a voltage signature on the SOI and polysilicon electrodes (b) and (c) respectively. We attribute these signals to the translocation of a *DNA* through the pore. (d) shows the difference between the poly and SOI electrodes. A STEM image of the 7nm diameter pore is shown in an inset of (d). We attribute the fluctuations in the difference voltage to charge on the *DNA*.

As shown in Figure 5, we observed a voltage transient on both the polysilicon (b) and SOI electrodes (c) that is nearly coincident with the blockade event observed in the current (a). We attribute these signals to the translocation of a single *DNA* molecule through the pore. The voltage signal associated with the translocation is on the level of ~1mV with a duration of about 200 seconds. Figure 5(d) represents the difference voltage measured between the SOI and polysilicon electrodes, showing a >1mV zero-to-peak signal level above a noise background of about 0.1mV-rms. The fluctuations observed in the difference voltage with about a 25 sec period are comparable to the response time associated with the 50kHz bandwidth of the Axon 700B amplifier used for the measurement. **This difference voltage signal represents the first measurement of a change in the polarization in a MOS capacitor due to the translocation of a single *DNA* molecule through it, and it provides us with an unequivocal identification of a translocation event since both probes show a voltage signature.** However, because of the large pore diameter, the shift in polarization may be associated with a combination of changes in the conformation of the molecule during the translocation, the transit of the phosphate backbone charge across the capacitor as well as the partial charges associated with the bases that comprise the molecule. As shown in Figure 6, the dipole moment associated with the charge distribution on each base is distinctive, but it lies in the plane of the

FIGURE 6. Dipole Moments of bases. Magnitude and vectors of dipole moments m. O-red, N-dark blue, C-light blue, and H white. Adob ed from Sponer.[133]

base with an orientation that is indicated by an angle relative to a reference line shown in the figure. Therefore, to facilitate the electrical detection of the polarization associated with each dipole, the base should be oriented perpendicular to the electrodes of a capacitor.
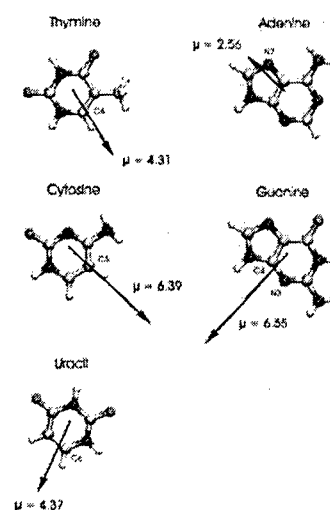
Molecular dynamic simulations of preliminary measurements of <1.25nm-radius pores for fields $<3.3 \times 10^6$V/cm indicate that we have already achieved this objective. Using molecular dynamic simulations (MD) to analyze our preliminary experimental findings with atomic detail, we have identified several key specifications of the transducer that affect the resolution and sensitivity: **(1)** the pore diameter and the electric field; **(2)** the oxide thickness; and **(3)** the molecular velocity. For example, as illustrated in Figure 6, we tested the voltage-driven permeability of *ssDNA* (58-mer) and *dsDNA* (58bp) through synthetic pores with effective radii of 0.5 ± 0.1nm, 0.95 ± 0.1nm and 1.5 ± 0.1nm in a Si_3N_4 membrane nominally 10nm thick. Following measurements of the electrolytic conductance that are used to characterize the pores, *DNA* in 10mM *TRIS-Cl* buffer at pH 8.5 was injected at the negative electrode. A voltage ranging from 100mV to 6V was applied across the membrane and the current through the nanopore was measured. While the voltage-driven translocations of the *DNA* across the membrane through the nanopore cause a temporary blockage in the open current through the pore, the narrow bandwidth (10-100kHz) of the amplifier used to measure the blockade may preclude the observation of all of the transients or noise fluctuations associated with interactions between the pore and the molecule that are shorter than 10-100μseconds. So, to unambigously establish that it permeates a nanopore, the minute amount of *DNA* near the positive electrode was amplified using *PCR* and analyzed by gel electrophoresis. Gel electrophoresis is a technique used to separate molecules according to size and charge across a span of gel using a driving force provided by a voltage applied at either end. After staining, the *DNA* in each lane can be seen as bands spread ccording to the length or molecular weight of the strand from one end of the gel to the other. Typical gel arrays are shown in Figure 7, along with a molecular weight reference denoted as "100bp ladder," which contains a spread of *DNA* a molecular weight. **Notice that the *ssDNA* collected at the positive electrode, denoted by (+)58-mer, is observed to permeate through all three pores, even the 0.5nm-radius pore, and gives the same amplified pattern as the *ssDNA* injected at the negative electrode, denoted by (-)58-mer. On the other hand, *dsDNA* does not permeate either the R_p=0.5nm or 1.0nm-radius pore, but it does permeate the R_p=1.5nm±0.1nm pore for a 200mV applied bias.**

Thus, the radius of the pore is a key specification, but so is the electric field in the pore. We also tested the voltage dependence of the permeability of *dsDNA* using two pores 1.0±0.1nm and

FIGURE 7. *(Top)* TEM images of pores (slightly out of focus) with apparent radii of the pores is R_p = 0.5 ± 0.1 nm and R_p = 1.0 ± 0.1 nm, and R_p = 1.5 ± 0.1 nm respectively in a 10 nm thick Si_3N_4 membrane viewed at 0° tilt angle. *(Bottom)* Gel arrays showing five horizontal lanes with fluorescent bands corresponding to the observation of 58-mer ss*DNA* and 58bp ds*DNA* at the positive (+) and negative (-) electrodes through the 0.5nm, 1.0nm and 1.5nm radius pores, respectively (with 100bp ladder as a reference) using a transmembrane bias of 200mV. ss*DNA* permeates all three pores, but ds*DNA* only translocates through the 1.5nm radius pore.

1.1±0.1nm in radius. The gel array in Figure 8(a) indicates that 58bp *dsDNA* can be forced through a 1nm-radius pore if the applied voltage is >2.75V. Notice that we only observe a fluorescent band in the lane corresponding to the positive
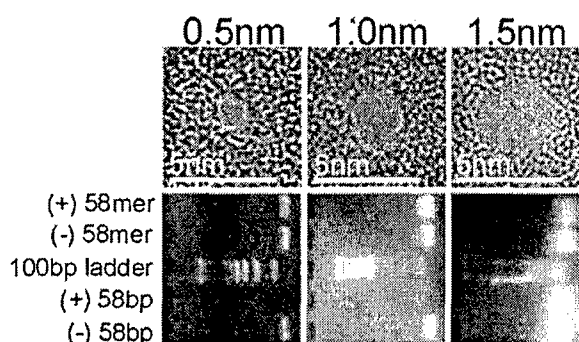
electrode, (+) 58bp, for an applied bias of 3V. We obtained a similar result for a 1.1±0.1nm-radius pore, but the observed threshold voltage was lower—58bp *dsDNA* permeates the pore for V> 2.25V. To establish the voltage threshold for translocation through a nanopore, the *DNA* copy number was measured by quantitative real-time PCR. The detection sensitivity allows us to enumerate the starting amounts of a nucleic acid template by analyzing the amount of *DNA* produced during each cycle of PCR. This is determined by identifying the cycle number at which the reporter dye emission intensity rises above background noise. This cycle number is identified as the threshold cycle (C_T). C_T is inversely proportional to the copy number of the target template; the higher the template concentration, the lower the threshold cycle measured. Two PCR primers were designed to amplify a 72bp region within a 622 base target sequence. A TaqMan® probe was designed mapping to this 72bp target sequence and labeled with a FAM reporter dye at the 5' end with a TAMRA quencher dye at the 3' end. During the amplification, the PCR primers and the probe all hybridize to the target sequence. During polymerization, the 5' exonuclease activity of the *DNA* polymerase cleaves the probe and the reporter dye is released resulting in increased fluorescence. The increase in fluorescence is proportional to the amount of target.

Figure 7(c) represents the results of qPCR analysis showing the copy number observed to permeate through 1±0.1nm and 1.1±0.1nm pores as a function of the applied voltage across the membrane. In correspondence with 2.75V threshold obtained from the gel array for 58bp, the 1nm-radius pore exhibits a threshold voltage of 2.5V for 622bp permeation. Similarly, the 1.1nm-radius pore shows a threshold voltage of 2V for 622bp permeation. The 0.25V discrepancy observed between the gel array and qPCR may be attributed to the difficulties associated with capturing and handling such a small number of copies.

For *ssDNA*, the steric constraints imposed by a 0.5nm-radius pore changes the *DNA* conformation during a translocation: nucleotide bases align with the pore axis and the distance between the consecutive nucleotides increases from 0.35 nm of unconstrained *DNA* to 0.7 nm. Figure 9(c) shows a typical configuration of the molecule inside a 0.5nm-radius pore with atomic detail; notice, in particular, the alignment of the bases along the axis of the pore. In order to investigate properties of the electrolyte around a *DNA* strand confined in a 0.5nm-radius pore simulations analogous to above were performed applying forces to both *DNA* and the electrolyte. In three independent simulations, imposing geometrical constraints led to a partial exclusion of water from the pore accompanied by condensation of potassium ions at specific sites along the *DNA* strand. Figure 9(a) shows the amount of water along the *DNA* strand confined in a 1nm diameter pore. Only a few water molecules were found at the narrowest part of the pore. Moreover, we find that potassium ions condense after partial de-wetting of the *DNA* strand at two sites: either between two consecutive phosphates of the *DNA* backbone or between backbone phosphate P and oxygen O of the nearby nucleotide base. Two such sites are indicated in Figure 9(c). *S*tretching the *DNA* and partial water exclusion are expected to result in a stronger sequence-dependent electrical signal compared to the signal from an unconstrained *DNA* because the molecule is stretched during the translocation, forcing the
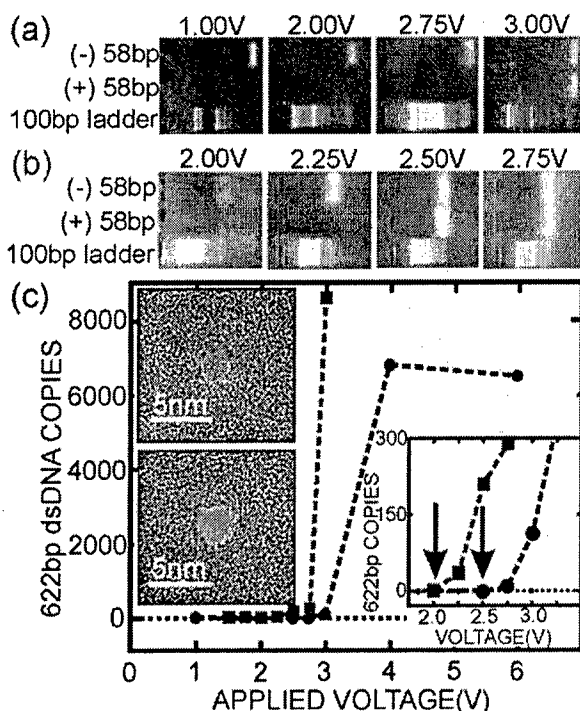

FIGURE 8. **(a)** Gel arrays containing 3 horizontal lanes with fluorescent bands indicating 58bp *dsDNA* found at the negative (-) and positive (+) electrodes in a bi-cell with a 1nm radius pore (along with a 100bp ladder for reference.) Notice that 58bp permeates the 1nm pore only for voltages V>2.75V. **(b)** Similar to (a) but instead using a 1.1nm radius pore. The 58bp permeates this pore only for V>2.25V. Figure **(c)** qPCR results obtained for the pores in (a) and (b) showing copy number versus voltage. *Upper left insets* TEM micrograph taken at 0° tilt for 1nm radius(blue) and 1.1nm radius(red). 622bp *dsDNA* permeates the 1nm pore for V>2.5V, and the 1.1nm pore for
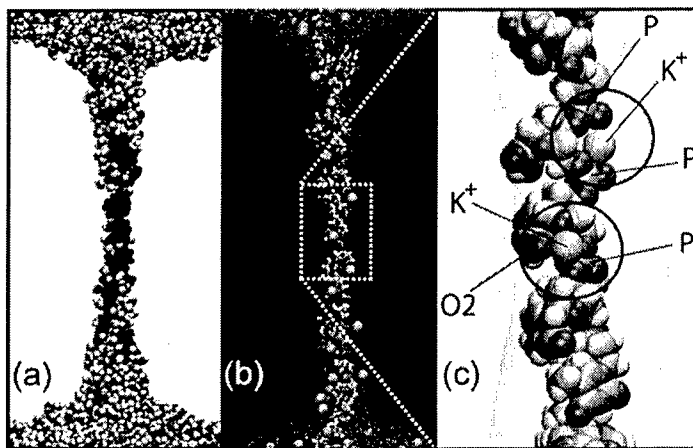

FIGURE 9. **Microscopic conformation of a 58-nucleotide *DNA* strand placed inside a 0.5nm-radius pore by Molecular Dynamics.** At the start of the simulation, a 58-nucleotide DNA strand floating in a 1M water solution of KCl was enclosed by a surface representing a 0.5-nm-radius pore. A 10 pN force pointing towards the pore center was applied to every DNA atom positioned outside of the pore surface. In a 1.5 ns simulation the radius of the pore was gradually reduced to 1.0 nm. Geometrical constraints induced changes in the *DNA* conformation: nucleotide bases aligned with the pore axis, the distance between consecutive nucleotides increased from 0.35 nm of unconstrained DNA to 0.7 nm. Water was found to be partially excluded from the narrowest part of the pore. Both DNA stretching and partial water exclusion are expected to result in a stronger sequence-dependent signal if compared to the signal from an unrestrained DNA

dipole moment associated with each base to be oriented along the pore axis nearly transverse to electrodes and maximizing the induce voltage on the capacitor electrodes. Moreover, while the *DNA* is in the pore, positive ions (K^+) become localized near the oxygen atoms on the backbone neutralizing the negative charge there and water molecules are expelled, eliminating the screening associated with it.

Thus, the 0.5nm-radius of the pore is a key specification for *ssDNA* for low voltage operation. On the other hand, 1.25nm-radius is a key specification for *dsDNA* for low voltage (<1.3V) operation. We simulated three systems: 0.7-, 1.0- and 1.5-nm-radii pores combined with one 58-bp *dsDNA* helix to compare with the low voltage results obtained experimentally at 200mV. To shorten the *dsDNA* translocation times to a practical duration, we chose to carry out most of these simulations at a 1.3V bias. First, we applied a uniform electric field across a 10.3-nm-thick Si_3N_4 membrane to drive a 58-basepair double helix through 0.7nm- and 1.0-nm-radius pores. The field induced a rearrangement of the ions and water that focused the electric field to the vicinity of the membrane, abolishing the field gradient in the bulk, and producing a 1.3 V transmembrane bias. Figure 10(a) shows a plot of the position of the *dsDNA* center of mass relative to the center of the Si_3N_4 membrane against the simulation time; circles and squares corresponds to the simulations carried our with the0.7nm and 1.0nm-radius pores. Within the first few nanoseconds of the simulations, the electric field drove *dsDNA* into the pores; the wider pore facilitated a faster translocation. Due to their conical shapes, both pores narrow towards the center of the membrane, which slowed down translocation of *DNA*. After about 4.5ns, the *DNA* translocation halted in both simulations *before DNA* arrived at the narrowest part of the pores. The snapshots included in the inset to Figure 10(a) illustrate the conformations of *dsDNA* at the end of these simulations. We noticed that *dsDNA* traveled a longer path inside the wider pore suggesting that the translocation halted at a particular cross-section. To ascertain if the translocation halted at the same cross-section in both pores, we plot in the insert of Figure 9(a) the local diameter of the pore around the first DNA base pair. In both simulations, the translocation of *dsDNA* halted when the pore narrowed to 1.25 ±0.1 nm-radius. From these simulations we conclude that the pores with a radius less than 1.25nm are impermeable to *dsDNA* for electric fields <1.3V/10nm, in excellent agreement with the experimental results shown in Figure 8.

To determine if a higher electric field could drive *dsDNA* through the same pores, we continued our simulations from the conformations shown in Figure 10(a), applying a 6V transmembrane bias. In Figure 10(b), we plot the position of the *dsDNA* center-of-mass against the simulation time with black and red symbols indicating the 1.3V and 6.0 V conditions. The results of these simulations suggest that *dsDNA* permeates both pores for a sufficiently high voltage. In the case of a 1.0nm-radius pore, the 6.0V bias deformed the *DNA* helix, shifting one of the *DNA* strands relative to the other by approximately one nucleotide, while preserving the hydrogen binding pattern between strands. Such stretching and shifting of the double helix reduces its effective diameter, allowing *dsDNA* to pass the constriction of the pore without unzipping. In the case of the 0.7nm-radius pore,

FIGURE 10. Results taken from MD simulations showing the center of mass of the 58bp *dsDNA* relative to the center of the Si_3N_4 membrane versus time. (a) A 1.3 V bias was applied to drive *dsDNA* into 0.7-nm-radius (circles) and 1.0-nm-radius (squares) pores. After about 4.5 ns, the translocation of *DNA* halted in both pores. The snapshots show conformations of *DNA* at the end of these simulations. The inset to (a) shows the radius of the pore cross-section near the first bp of *dsDNA* inside the 0.7- (circles) and 1.0-(squares)-nm-radii pores. The translocation of *dsDNA* halts when the pore narrows to 1.25±0.1nm. (b) Translocations of 58bp *dsDNA* through 0.7nm(circle), 1.0nm(square), and 1.5nm(triangle) radius pores. Black and red symbols reflect the magnitude of the applied bias: 1.3 and 6.5 V, respectively. The snapshot on the left illustrates the stretch *dsDNA* permeating 1.0-nm radius pore at 6.5V bias. This pore was not observed to conduct *dsDNA* at 1.3V bias. The middle snapshot shows the final conformation of *dsDNA* after passing through the narrowest part of the 1.5nm radius pore at 1.3 V. Snapshot on the right illustrates the unzipping of the *dsDNA* strands inside the 0.7nm-radius pore at 6.5 V. (c) *dsDNA* permeates a 1.0nm radius pore for voltages >3.2V. The inset

the 6.0V bias unzipped *dsDNA* before it reached the narrowest part of the pore. After denaturing, one of the two strands was observed to fit into the 0.7nm-radius pore. In contrast to the 0.7nm- and 1.0nm-radius pores, we found that *dsDNA* permeates a 1.5nm-radius pore at a bias of 1.3 V. In Figure 10(b), the *dsDNA* center of mass is plotted against the
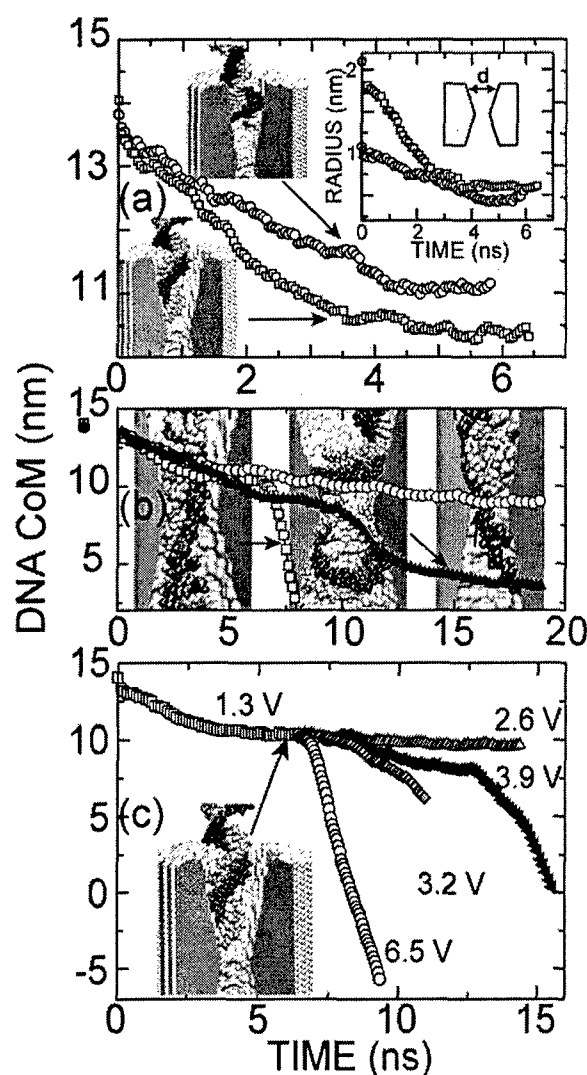
simulation time (filled triangles). Within the first 5ns, the field drove *dsDNA* into the 1.5nm-radius pore with a speed comparable to that inside the 0.7nm- (circles) and 1.0nm-radius(squares) pores. In the 1.5nm pore simulation, however, the translocation of *DNA* did not halt before reaching the center of the membrane. Instead, after about 11ns, one end of the *DNA* helix passed through the 1.5-nm-constriction in the pore. Shortly following that, this end adhered to the surface of Si_3N_4 on the other side of the pore (z<0). Driven by the field, the rest of the *DNA* helix continued the move through the pore, deforming the double helix of *DNA* into a loop, as shown in Figure 10(b). A compete translocation of this type was reported earlier.[10]

Finally, to establish the threshold field and subsequently the force required to stretch 58bp *dsDNA* and drive it through the pore, we continued our simulation of the 1nm-radius pore from the conformation observed at 6nsec with a bias of 1.3V as shown in Figure 10(c). In Fig. 10(c) we plot the position of the *dsDNA* center-of-mass against the simulation time for biases ranging from 1.3 to 6.5V. These results indicate that *dsDNA* permeates a 1.0nm-radius pore only for voltages ≥3.2V. **This prediction is in excellent agreement with the 3V threshold measured in a 1nm-radius pore using precisely the same *dsDNA* molecule shown in Figure 8(a), and succinctly illustrates accuracy of the MD model.** At 3.2V, we evaluated the net force on a nucleotide at the leading edge of the molecule in the 1.0nm constriction and found that 60±3pN was sufficient to shift one of the *DNA* strands relative to the other by approximately one nucleotide, allowing *dsDNA* to pass the constriction without unzipping. This value is consistent with the force corresponding to the stretch-transistion measured in single molecule spectroscopies that are used to infer the average elastic properties of long (48kbp~16.3 m) molecules from force-extension measurements. When subjected to a force >*10pN*, the molecule starts to deform, stretching the double helix. But it is especially remarkable that near *60pN* a dramatic and sharp transition occurs—the double helix changes from 107% to nearly 170% of the length of *B-DNA* over a few picoNewtons.[3,4] The distance between successive bases in the stretched *DNA* is 0.7nm, which is about a factor of 2 larger than the normal rise per base of 0.34nm.

In pursuit of the voltage signal derived from the dipole associated with individual bases in *ssDNA*, we are currently exploring pores with a 0.7nm-radius in a capacitor membrane. Likewise, we are examining pores with a 1nm-radius for dsDNA and a 2nm-radius for alkaline phosphatase. We have obtained preliminary measurements of the voltage and current signals corresponding to the translocation of a *ssDNA* molecule through a structure similar to that shown in Figure 1, consisting of a thin 4.2nm oxide sandwiched between two heavily doped (n-type) electrodes: one made from polysilicon 18nm thick and another from crystalline silicon 22nm thick, using a pore with a radius <0.75nm. We injected 150-mer *ssDNA* into 1M *KCl* electrolyte near the Ag-AgCl anode. While monitoring the ionic current through the pore under an applied bias between the *AgCl* electrodes of 200mV, we observed transients associated with single ss*DNA* molecules temporarily blocking the electrolytic current through the pore similar to those shown in Figure 11(a). Concurrent with the transients observed in the current, we recorded the voltage on the SOI and polysilicon electrodes, as well. As shown in Figure 11, we observed a voltage signature on both the polysilicon (b) and SOI electrodes (c) that is nearly coincident with an event observed in the current (a). We attribute these signals to the
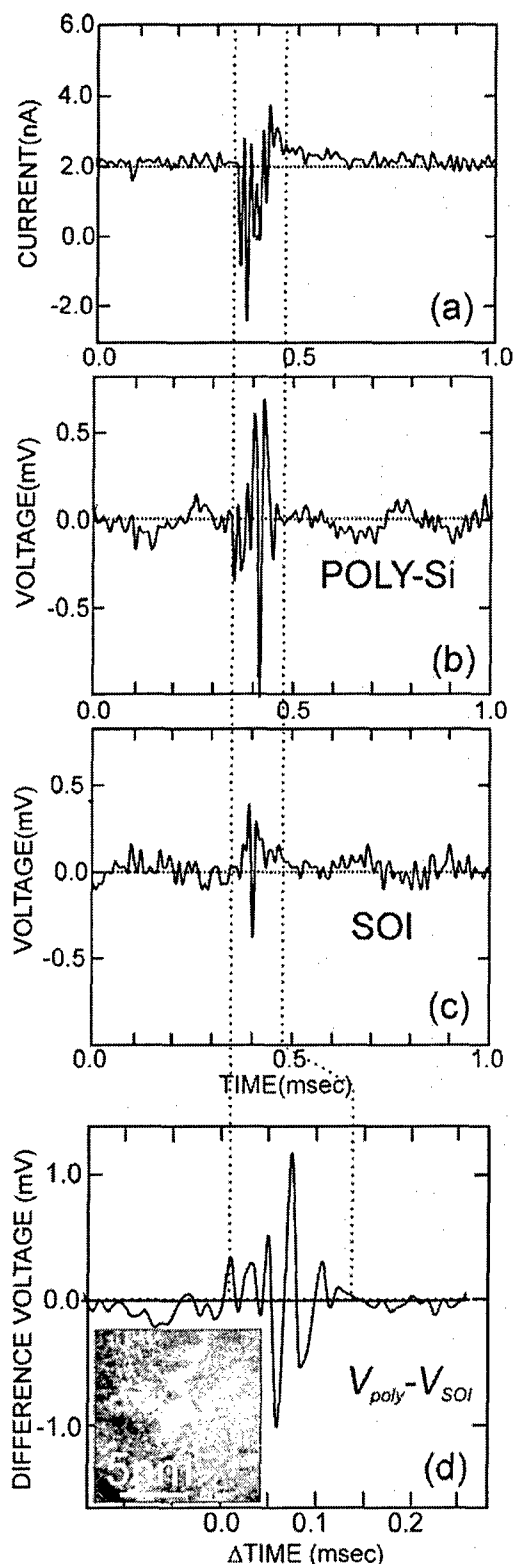

FIGURE 11. Translocation through a 7nm Diameter Pore in a Capacitor. Corresponding to a transient in the current (a), we observe a voltage signature on the SOI and polysilicon electrodes (b) and (c) respectively. We attribute these signals to the translocation of a *DNA* through the pore. (d) shows the difference between the poly and SOI electrodes. A STEM image of the 7nm diameter pore is shown in an inset of (d). We attribute the fluctuations in the difference voltage to charge on the *DNA*.

translocation of a single ssDNA molecule through the pore. The voltage signal associated with the translocation is on the level of ~1mV with a duration of about 200 seconds. Figure 11(d) represents the difference voltage measured between

the SOI and polysilicon electrodes, showing a >1mV zero-to-peak signal level above a noise background of about 0.1mV-rms. While this difference voltage signal demonstrates the feasibility of using a nanopore in a membrane comprised of an MOS capacitor as an electrical transducer, we did not observe a signal that is unique to this 150-mer molecule in these preliminary experiments, nor is the time-resolution sufficient to detect a single nucleotide.

From the MD analysis given above, we infer another key specification of the nanopore transducer: the thickness of the SiO_2 insulator separating the electrodes forming the capacitor. Ostensibly, 0.7nm SiO_2 thickness would be required to achieve the spatial resolution for sequencing ssDNA (and dsDNA in the stretched configuration) with a 0.5nm-radius pore. We have already fabricated capacitors with oxides this thin, but the quantum mechanical tunneling current across the electrodes is about about 12 A for 1V applied across a 2 mx2 m capacitor. (This leakage current does not prohibit an ac-impedance measurement of the change in polarization since the in-phase (conductive) and quadrature (capacitive) components to the signal can be easily discriminated.) However, our simulations indicate that we can use a thicker oxide (up to 2nm) without compromising resolving power. For example, Figure 12 illustrates an estimate of the voltage signal induced on two ideal electrodes located on either side of a 0.5nm-radius pore as bases in ssDNA are forced through a 2nm thick insulator. The position of the two electrodes is represented by the blue and red annuli in the figure; they are separated by 2nm along the pore-axis. The recorded voltages are plotted versus time on the top figure, while the bottom figure indicates the dipole moment of the DNA bases projected along the pore axis. During this simulation 14 bases translocated through the pore. The letters above the top figure represent the sequence of bases confined between the electrodes at a specific instant in time. Notice the regular variations in the voltage on both electrodes, which are indicative of the nucleotides translocating through the pore. For example, near 0.4nsec we find three oscillations in the voltage corresponding to a shift in the position of three nucleotides in the polymer from C to G to T and finally to A. These oscillations are observed even if the molecule is forced through the pore at a different rate, indicating that they are independent of the particular molecular conformation. **The oscillations in the voltage, which correlate with the passage of a nucleotide between the electrodes, indicate that it may be possible to resolve the translocation of individual nucleotides in a 0.5nm-radius pore, even if the electrodes are spaced 2nm apart.** The corresponding changes in the calculated dipole moment taken from a sum over all the partial charges in the section of the molecule between the probes might be used to unravel the chemical sequence, but we have not yet identified an unequivocal chemical signature in the voltage data. In particular, notice from Figure 12(c) that the level of noise associated with the detection of the dipole is expected to be comparable to the signal. (Similar results were obtained, using a voltage >3V in conjunction with a 1nm-radius pore to stretch a dsDNA molecule to detect the electrical signals associated with the passage of base-pairs with electrodes spaced 2nm apart with similar signal-to-noise.)

To amplify the electrical signal over sufficient bandwidth to detect a nucleotide permeating the pore, we plan to integrate an MOSFET amplifier directly onto the same chip with the nanopore sensor. As shown above, MD simulations
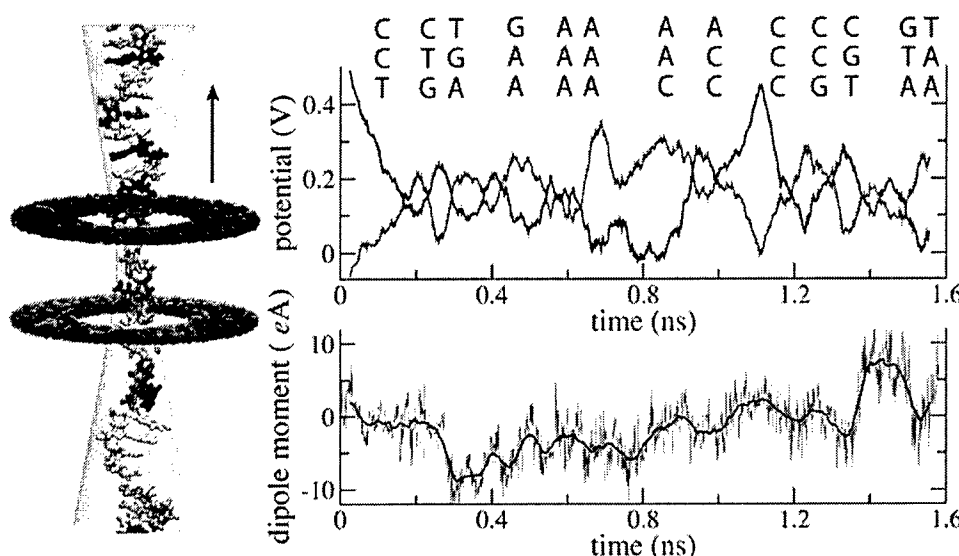

FIGURE 12. Induced Voltage and Average Dipole Moment of DNA Translocating though a 1nm Pore. The voltage induced by DNA translocation through the pore was measured at two disk-like electrodes shown in blue and red. The recorded signals are plotted versus time on the top figure. The bottom figure indicates the dipole moment of DNA bases projected along the pore axis. During this simulation 14 bases translocated through the pore. The letters above the top figure represent the sequence of bases confined inside the pore. The regular oscillations in the voltage are associated with single nucleotides translocating through the pore. Similar features are observed even if the molecule is pulled through the pore at a faster rate (corresponding to a different molecular configuration.)

indicate that the translocation of a 58-mer strand of ssDNA requires <1msec and in some cases <10nsec (for the fields used in the simulations), which translates to a transition rate of 1 nucleotide in the range 50psec-10nsec for a raw read or a maximum bandwidth of 20GHz. For 20dB of gain at this frequency the cut-off frequency of the amplifier should be nearly 200GHz. We have produced high-gain, low noise, wide-bandwidth MOSFET amplifiers with a process flow that is compatible with the production of the capacitor membranes, which is an essential aspect of our proposal. Figure 13(a) shows a TEM cross-section through a 30nm gate length nMOSFET transistor amplifier along with the frequency response measured in a similar 50nm and 30nm device with two finger gates 5μm and 40 μm wide, respectively.
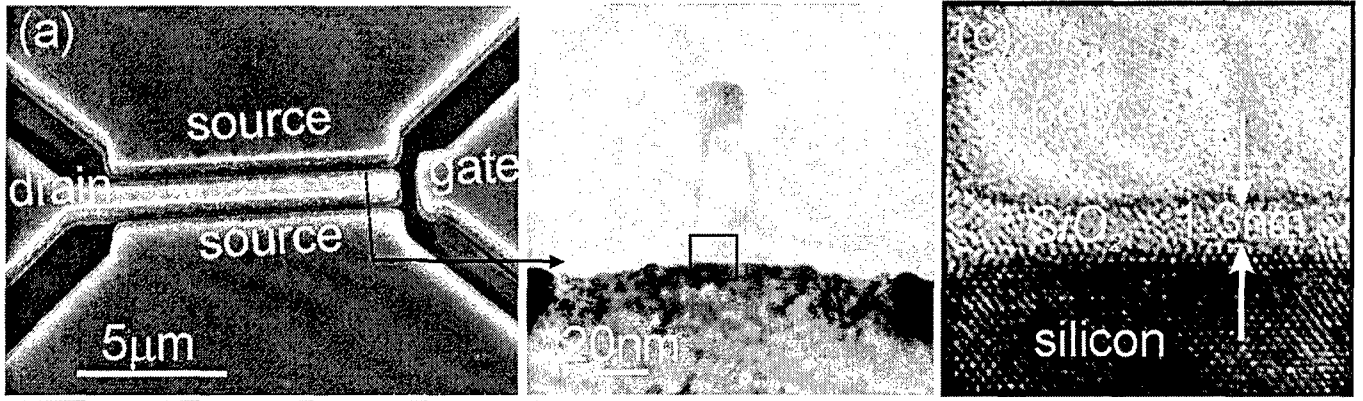
Figure 13. (a) A scanning electron micrograph of a two-leg MOSFET. The dashed line indicates the region shown in cross-section in Fig. (b). (b) A transmission electron micrograph (TEM) of one finger of a nominally 30nm gate length nMOSFET with a 1.3nm thick gate oxide. The gate is comprised of a heavily doped polysilicon layer 95nm thick with a CoSi$_2$ strap. The 40nm sidewalls consist of a 10nm thick oxide layer beneath 30nm of silicon nitride. A magnified view of the area outlined in (b) is shown in detail in (c).

Two figures-of-merit for the high frequency performance are the cut-off frequency associated with short-circuit current gain, f_T, and the maximum frequency of oscillation, f_{max}:

$$f_T \approx \frac{g_m}{2\pi(C_{gs}+C_{gd})} \sim \frac{1}{L_g^2}, \quad f_{max} \approx \frac{f_T}{2\sqrt{R_g(g_{ds}+f_T C_{gd})}} \sim \frac{1}{W}$$

where g_m is the transconductance and C_{gs} and C_{gd} are the gate-to-source and gate-to-drain capacitances, R_g is the (lumped) gate resistance and g_{ds} is the output conductance. f_T is a key measure of performance since f_{max} is proportional to it. Ostensibly, improvements in f_T follow from scaling of the channel length or gate length L_g. We have witnessed the progressive increase[1-3] of f_T to a world record of f_T =290GHz that we recently measured in a 30nm gate length nMOSFET as shown in Figure 14(a), which is comparable to observations in sub-100nm InP[4] HEMTs, but still inferior to reports on SiGe[5] and InP/InGaAs[6-8] HBTs. On the other hand, in MOS technology, f_{max} generally lags behind f_T. This disparity between f_T and f_{max} can be accounted for by parasitics,[9] such as R_g and g_{ds}, that are not optimized in a core CMOS manufacturing process for high frequency performance. Recently, using a transistor unit cell consisting of a multi-finger, folded gate geometry, which minimizes the gate resistance and the drain capacitance,[10] Kuhn et al.[1] achieved a substantial improvement in f_{max} to 248GHz for 70nm gate length nMOSFET with a standard digital process flow. Following their lead, we used a multi-finger gate geometry, but for economy we did not optimizing the number of gate fingers. Figure 14(c) illustrates f_{max}=135GHz, in our preliminary work achieved with 2 fingers (the optimum number of fingers is usually between 4-6, which requires a much more expensive second layer of metal processing.) Despite the poor comparison to current 70nm, f_{max}=135GHz represents more than sufficient power gain for operation at frequencies <20GHz. Finally, to make effective use of digital CMOS technology for RF, the noise figure, F_{min}, also has to be minimized with an acceptable associated gain. Like f_T, F_{min} should improve (diminish) with each technology generation according to:

$$F_{min} \approx 1 + K\frac{f}{f_T}\sqrt{g_m(R_g+R_s)}$$

where K is a constant that depends on the technology. Just like f_{max}, F_{min} also depends on parasitic elements that are sensitive to the gate bias and geometry. We find that the noise figure ranges from 1.3-3dB for low frequency <5GHz operation. The measured input voltage noise is e_n=3.2nV/√Hz

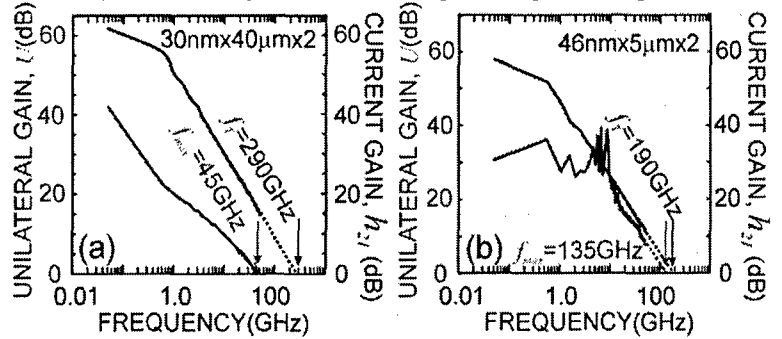**FIGURE 14.** Frequency response of the current and unilateral gain measured in (a) 30nmx40μmx2 and (b) 46nmx5μmx2 nMOSFETs. f_T and f_{max} were obtained at Vds=2V by extrapolating S-parameter-measurements in the 40-50GHz range using a slope of 20dB/decade. Despite the degradation in f_T relative to the device in (a), f_{max} improves substantially with an increase in the channel length and a decrease in channel width.